Solar Phys (2017) 292:79
DOI 10.1007/s11207-017-1102-7

Investigation of the Geoeffectiveness of Disk-Centre Full-Halo Coronal Mass Ejections

Dheyaa Ameri[1,2] · **Eino Valtonen**[1]

Received: 6 September 2016 / Accepted: 27 April 2017

Abstract We studied the occurrence and characteristics of geomagnetic storms associated with disk-centre full-halo coronal mass ejections (DC-FH-CMEs). Such coronal mass ejections (CMEs) can be considered as the most plausible cause of geomagnetic storms. We selected front-side full-halo coronal mass ejections detected by the *Large Angle and Spectrometric Coronagraph* onboard the *Solar and Heliospheric Observatory* (SOHO/LASCO) from the beginning of 1996 till the end of 2015 with source locations between solar longitudes E10 and W10 and latitudes N20 and S20. The number of selected CMEs was 66 of which 33 (50%) were deduced to be the cause of 30 geomagnetic storms with Dst ≤ -50 nT. Of the 30 geomagnetic storms, 26 were associated with single disk-centre full-halo CMEs, while four storms were associated, in addition to at least one disk-centre full-halo CME, also with other halo or wide CMEs from the same active region. Thirteen of the 66 CMEs (20%) were associated with 13 storms with -100 nT $<$ Dst ≤ -50 nT, and 20 (30%) were associated with 17 storms with Dst ≤ -100 nT. We investigated the distributions and average values of parameters describing the DC-FH-CMEs and their interplanetary counterparts encountering Earth. These parameters included the CME sky-plane speed and direction parameter, associated solar soft X-ray flux, interplanetary magnetic field strength, B_t, southward component of the interplanetary magnetic field, B_s, solar wind speed, V_{sw}, and the y-component of the solar wind electric field, E_y. We found only a weak correlation between the Dst of the geomagnetic storms associated with DC-FH-CMEs and the CME sky-plane speed and the CME direction parameter, while the correlation was strong between the Dst and all the solar wind parameters (B_t, B_s, V_{sw}, E_y) measured at 1 AU. We investigated the dependences of the properties of DC-FH-CMEs and the associated geomagnetic storms

Earth-affecting Solar Transients
Guest Editors: Jie Zhang, Xochitl Blanco-Cano, Nariaki Nitta, and Nandita Srivastava

✉ D. Ameri
dheyaa.a.ameri@utu.fi

✉ E. Valtonen
eino.valtonen@utu.fi

[1] Department of Physics and Astronomy, University of Turku, 20014 Turku, Finland

[2] Department of Physics, University of Basra, Karmat Ali B.P49, Basra, Iraq

Published online: 12 June 2017

on different phases of solar cycles and the differences between Solar Cycles 23 and 24. In the rise phase of Solar Cycle 23 (SC23), five out of eight DC-FH-CMEs were geoeffective (Dst ≤ -50 nT). In the corresponding phase of SC24, only four DC-FH-CMEs were observed, three of which were nongeoeffective (Dst > -50 nT). The largest number of DC-FH-CMEs occurred at the maximum phases of the cycles (21 and 17, respectively). Most of the storms with Dst ≤ -100 nT occurred at or close to the maximum phases of the cycles. When comparing the storms during epochs of corresponding lengths in Solar Cycles 23 and 24, we found that during the first 85 months of Cycle 23 the geoeffectiveness rate of the disk-centre full-halo CMEs was 58% with an average minimum value of the Dst index of -146 nT. During the corresponding epoch of Cycle 24, only 35% of the disk-centre full-halo CMEs were geoeffective with an average value of Dst of -97 nT.

Keywords Coronal mass ejections, interplanetary · Magnetosphere, geomagnetic disturbances · Solar wind, disturbances

1. Introduction

Geomagnetic storms are produced when mass and momentum are transferred from the solar wind into the magnetosphere, as a consequence of magnetic reconnection of an interplanetary (IP) magnetic structure with Earth's magnetic field. The major single factor contributing to the occurrence of magnetic storms is the existence of a strong, long-duration southward magnetic field component (B_s) in the IP magnetic structure (Gonzalez *et al.*, 1994; Tsurutani and Gonzalez, 1997). Coronal mass ejections (CMEs), corotating interaction regions, and Alfvenic turbulence in the solar wind are possible sources of B_s in the IP magnetic field (Gonzalez *et al.*, 1994; Lindsay, Russell, and Luhmann, 1995; Xu *et al.*, 2009; Zhang and Moldwin, 2014, and references therein). Various indices can be used to measure the level of geomagnetic activity and to assess the severity of magnetic storms (Mayaud, 1980). The Dst index represents the average change in the horizontal component of Earth's magnetic field (in units of nT) caused by a geomagnetic storm at four low latitude stations and depends on the strength of the magnetospheric ring current. Loewe and Prölss (1997) classified geomagnetic storms into five groups based on the minimum value of Dst: weak (-50 nT $<$ Dst ≤ -30 nT), moderate (-100 nT $<$ Dst ≤ -50 nT), strong (-200 nT $<$ Dst ≤ -100 nT), severe (-350 nT $<$ Dst ≤ -200 nT), and great (Dst ≤ -350 nT). Weak and moderate storms can be caused by both CMEs and corotating interaction regions (*e.g.* Xu *et al.*, 2009; Yakovchouk *et al.*, 2012). However, the more intense storms are primarily caused by CME-driven interplanetary disturbances (Gosling *et al.*, 1991) (see also Zhang *et al.*, 2007; Richardson and Cane, 2012).

Only those CMEs which are directed towards Earth can cause geomagnetic storms. Therefore, front-side full-halo CMEs are the most probable candidates. Many authors have investigated the geoeffectiveness of halo CMEs and searched for parameters of halo CMEs that best correlate with the occurrence and strength of geomagnetic storms. In early studies of CMEs observed by the *Large Angle and Spectrometric Coronagraph* onboard the *Solar and Heliospheric Observatory* (SOHO/LASCO) (Brueckner *et al.*, 1995) both full-halo and partial halo CMEs were often included in the statistics (*e.g.* Cane, Richardson, and St. Cyr, 2000; Webb *et al.*, 2000; Wang *et al.*, 2002; Zhang *et al.*, 2003) and varying results were obtained for the percentage of geoeffective halo CMEs. It was realised that in order to predict their geoeffectiveness, it was important to know the actual direction of CMEs and better understand the propagation of CMEs between the Sun and the Earth (Cane, Richardson, and

St. Cyr, 2000). It was also found that the source locations of geoeffective halo CMEs had a western bias due to the solar magnetic field spiral structure (Wang *et al.*, 2002; Zhang *et al.*, 2003). Zhao and Webb (2003) investigated time variations of the storm effectiveness of front-side full-halo CMEs from 1996 to 2000. During the early ascending phase of the solar cycle nearly all the CMEs were associated with geomagnetic storms (Dst < -50 nT), but towards the solar cycle maximum the storm effectiveness reduced to 40%. As a possible explanation for the lower storm effectiveness near solar maximum they suggested the origin of the CMEs from source regions under the bipolar coronal streamer belt at the base of the heliospheric current sheet leading to weaker chance of generating sustained southward magnetic field structures at 1 AU due to increased inclination of the heliospheric current sheet during solar maximum. Using a large sample of halo CMEs from 1996 – 2005, Gopalswamy, Yashiro, and Akiyama (2007) found that 75% of disk halo CMEs were geoeffective (Dst < -50 nT). Source location and speed of the CMEs were the most important parameters explaining geoeffectiveness, while there was no significant difference in flare size among geoeffective and nongeoeffective halo CMEs.

Relatively good correlations between the linear sky-plane speed of CMEs and the strength of the associated geomagnetic storms have been reported by, *e.g.*, Srivastava and Venkatakrishnan (2004), Kim *et al.* (2005), Gopalswamy (2009), Vasanth and Umapathy (2013), and Shanmugaraju *et al.* (2015). When determining probability distributions of the Dst index as a function of CME and solar flare parameters, Dumbović *et al.* (2015) concluded that faster CMEs had higher probability of producing strong geomagnetic storms and slow CMEs (< 600 km s^{-1}) were not likely to produce intense (Dst < -200 nT) storms, unless involved in interaction with a faster CME. The initial speed of the CMEs did not, however, alone determine the CME geoeffectiveness probability. Gopalswamy *et al.* (2015a) studied properties of magnetic clouds during Solar Cycles 23 and 24 and found that the product of the magnetic cloud flow speed and the southward component of the cloud magnetic field was the primary factor determining the strength of geomagnetic storms. Michalek *et al.* (2006) and Michalek, Gopalswamy, and Yashiro (2007) have reported based on the CME cone models (Michałek, Gopalswamy, and Yashiro, 2003; Michalek, 2006) that using the space speed of CMEs instead of the projected sky-plane speed the correlation with storm strength is stronger.

In order to estimate the propagation direction of front-side halo CMEs, Moon *et al.* (2005) defined an earthward-direction parameter based on CME asymmetries. Kim *et al.* (2008) used this parameter in studying the geoeffectiveness of 486 front-side halo CMEs and showed that CMEs with large direction parameters had a high association with geomagnetic storms. With increasing direction parameter, the geoeffectiveness also increased. Similar results were reported by Shanmugaraju *et al.* (2015) for 40 halo CMEs at the rising phase of Solar Cycle 24. In an investigation of 50 front-side full-halo CMEs, Lee *et al.* (2014) found the best correlation between Dst and combined parameters, which involved the CME radial speed together with either the CME direction parameter or the angle between the CME cone axis and the plane of the sky as defined in the cone model of Michałek, Gopalswamy, and Yashiro (2003). Lee *et al.* (2014) concluded that also the longitude and magnetic field orientation of a front-side full-halo CME source region played a significant role in predicting geomagnetic storms.

In this article, we investigate the characteristics of geomagnetic storms associated with a spatially well constrained set of full-halo CMEs launched from close to the central meridian of the Sun during the period 1996 – 2015. Such CMEs can be considered as the most plausible cause of geomagnetic storms. In Section 2 we describe the selection of data used in this investigation. Section 3 presents statistics of the selected CMEs and the associated geomagnetic storms. In Section 4 we discuss the dependence of the geomagnetic storm strengths on

the properties of disk-centre full-halo CMEs. The dependence of geomagnetic storms on the solar wind conditions associated with the disk-centre full-halo CMEs is discussed in Section 5. In Section 6 we compare the geomagnetic activity associated with disk-centre full-halo CMEs during Solar Cycles 23 and 24. Section 7 summarises the results and presents the conclusions.

2. Data and Event Selection

The SOHO/LASCO (Brueckner *et al.*, 1995) catalogue of halo CMEs[1] (Gopalswamy *et al.*, 2010b) was used to select disk-centre full-halo CMEs (DC-FH-CMEs). The catalogue contains 697 halo CMEs observed between 1996 and 2015 of which 394 are front-side with the source locations given in the catalogue in heliographic coordinates. Halo CMEs originating from source locations between longitudes E10 and W10 and latitudes N20 and S20 are defined in this article as disk-centre full-halo CMEs. In the latitudes of the selected CMEs, the solar B0 angle, the angle between the solar equator and the ecliptic plane, was taken into account, *i.e.* the event selection is based on latitudes measured from the ecliptic plane. We found 66 DC-FH-CMEs, which represent 16.8% from the total number of front-side halo CMEs for the investigated period. The selected disk-centre full-halo CMEs with their relevant properties are presented in Table 6 in the Appendix.

Following Gopalswamy, Yashiro, and Akiyama (2007) we define that a CME is geoeffective, if it is followed by a minimum value of Dst ≤ -50 nT. We further divide the CMEs in moderately geoeffective, if -100 nT $<$ Dst ≤ -50 nT, and strongly geoeffective, if Dst ≤ -100 nT. Also, in this article we use a simplified version of the storm classification of Loewe and Prölss (1997) and apply Dst ≤ -50 nT as the limit for a geomagnetic storm with -100 nT $<$ Dst ≤ -50 nT and Dst ≤ -100 nT being moderate and strong geomagnetic storms, respectively. The Dst values were obtained from the World Data Center for Geomagnetism, Kyoto.[2]

Based on the launch times and linear speeds of the CMEs given in the SOHO/LASCO halo CME catalogue, we estimated the arrival times of the corresponding interplanetary CMEs (ICMEs) at 1 AU by using the drag-based model of Vršnak *et al.* (2013) (see also Shanmugaraju and Vršnak, 2014). The model parameters were selected according to the guidelines given by Vršnak *et al.* (2013). We then associated a DC-FH-CME with a geomagnetic storm, if a storm with a minimum Dst ≤ -50 nT was found within a ± 24 hour time window from the predicted arrival time of the corresponding ICME (see, Kim *et al.*, 2005; Shanmugaraju *et al.*, 2015; Vasanth *et al.*, 2015). In various cases, the DC-FH-CME storm association was done in the following way. If a storm occurred within the ± 24 hour time window from the predicted arrival time of a DC-FH-CME (more precisely its interplanetary counterpart) and if this storm was not in the arrival time window of any other front-side halo or partial halo CME, then the DC-FH-CME was the cause of the storm. If a storm occurred in the arrival time windows of several CMEs (at least one DC-FH-CME and possibly one or more other halo or wide CMEs) and if the time order of the CME arrivals was the same as their launch time order from the Sun, then the CME which had the arrival time closest to the Dst minimum time was taken as the cause of the storm. If within these time windows there were also several storms, we selected the CME–storm pairs according to their temporal sequence (see also Kim *et al.*, 2005). If the initial speeds and height–time plots of

[1] http://cdaw.gsfc.nasa.gov/CME_list/HALO/halo.html.

[2] http://wdc.kugi.kyoto-u.ac.jp/dstdir/.

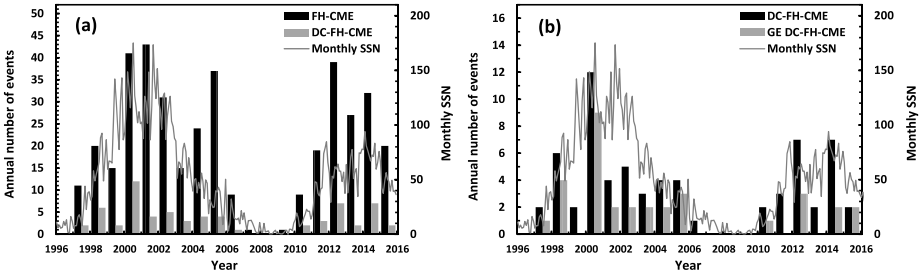

Figure 1 (a) The annual number of all front-side full-halo CMEs (FH-CME) compared with the disk-centre full-halo CMEs (DC-FH-CME) as a function of time for the period investigated (left-hand vertical scale). (b) As (a), but for all disk-centre full-halo CMEs and for geoeffective DC-FH-CMEs. For comparison, the monthly average sunspot number is also shown (right-hand vertical scale).

successive CMEs and their predicted arrival times indicated that the successive CMEs might have merged together on their way to 1 AU it was not possible to determine which of the two or more CMEs specifically caused the storm. In this case all involved DC-FH-CMEs were considered to be geoeffective (see Zhang *et al.*, 2003; Gopalswamy, Yashiro, and Akiyama, 2007).

To assist associating DC-FH-CMEs with geomagnetic storms (Dst ≤ -50 nT), we used several existing catalogues and previous publications, such as the list of near-Earth interplanetary coronal mass ejections[3] of Richardson and Cane (2010), the interplanetary shock list of Gopalswamy *et al.* (2010a), and the list of solar and interplanetary sources of major geomagnetic storms of Zhang *et al.* (2007). In addition, we used the catalogue of high-speed solar wind streams of Xystouris, Sigala, and Mavromichalaki (2014) to distinguish high-speed solar wind streams from coronal holes as a possible cause of the storms.

3. Event Statistics

The annual number of all front-side full-halo CMEs (FH-CMEs) is compared with that of the disk-centre full-halo CMEs in Figure 1a. During Solar Cycle 23 (SC23) (May 1996 – November 2008), the maximum number of FH-CMEs occurred in 2001, while the maximum number of disk-centre full-halo CMEs occurred in 2000. During the on-going Solar Cycle 24 (SC24) (from December 2008 till end of December 2015), the maximum number of FH-CMEs occurred in 2012, while there were equal numbers of disk-centre full-halo CMEs in 2012 and 2014. The number of DC-FH-CMEs represents 17.4% (43 out of 247) and 15.6% (23 out of 147) from the total number of front-side full-halo CMEs in SC23 and SC24, respectively. In total, during the two solar cycles, 50% (33 out of 66) of the DC-FHC-MEs were geoeffective. The annual number of geoeffective DC-FH-CMEs is presented in Figure 1b. The largest numbers of geoeffective events occurred in 2000 in Solar Cycle 23 and in 2012 in Cycle 24. In 1996, 1999, 2006 – 2009, 2011, and 2013 there were no geoeffective DC-FH-CMEs, while in 2015 all events were geoeffective. The annual numbers of both FH-CMEs and DC-FHC-MEs follow reasonably well the monthly average sunspot number too (Figure 1).

[3] http://www.srl.caltech.edu/ACE/ASC/DATA/level3/icmetable2.htm.

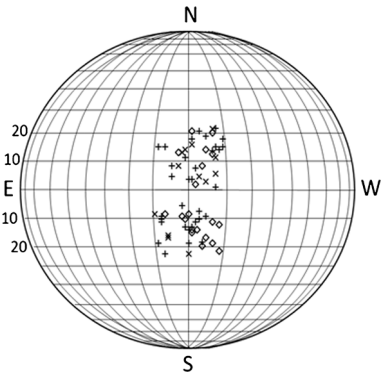

Figure 2 Heliographic locations of the 66 disk-centre full-halo CMEs during 1996 – 2015. The plus, cross, and diamond symbols correspond to nongeoeffective, moderately geoeffective, and strongly geoeffective events, respectively. Note that when the B0 angle is taken into account, all events fall within the range $[-20°, +20°]$ from the ecliptic.

Table 1 Properties of disk-centre full-halo CMEs from different disk-centre quadrants.

Quadrant	S-GE[a]	M-GE[b]	Dst ≤ −50 nT	Average Dst (nT)	Non-geoeffective	Total number	Average CME-speed ($km\,s^{-1}$)	Average[c] DP
SW	10 (50%)	1 (5%)	11 (55%)	−176	9 (45%)	20	761	0.72
NW	5 (25%)	5 (25%)	10 (50%)	−125	10 (50%)	20	938	0.56
SE	4 (25%)	4 (25%)	8 (50%)	−112	8 (50%)	16	616	0.58
NE	1 (10%)	3 (30%)	4 (40%)	−108	6 (60%)	10	651	0.56

[a]Strongly geoeffective.

[b]Moderately geoeffective.

[c]Average direction parameter (see Section 4).

The solar source locations of the disk-centre full-halo CMEs are shown in Figure 2. CMEs from the western regions within the longitude range [W00, W10] and latitude range [S20, N20] (B0 taken into account) are much more frequent (40 out 66) than the events from the eastern regions (longitudes [E00, E10] and latitudes [S20, N20]) (26 out of 66). We divided the source locations further into four quadrants: south-western (SW) within the latitude range [S00, S20] and longitude range [W00, W10], north-western (NW) within [N00, N20] and [W00, W10], south-eastern (SE) within [S00, S20] and [E00, E10], and north-eastern (NE) within [N00, N20] and [E00, E10]. The numbers of geoeffective and nongeoeffective CMEs, the average values of associated minimum Dst, the average CME speeds, and the average direction parameters for the DC-FH-CMEs in these four quadrants are presented in Table 1. Clearly, the CMEs originate more frequently from the SW and NW quadrants than from the SE and NE quadrants. Also, CMEs from the SW and NW quadrants are relatively slightly more frequently geoeffective than those from SE and NE. This is in accordance with earlier findings (Wang *et al.*, 2002; Zhang *et al.*, 2003). CMEs from the SW quadrant are frequently (50%) strongly geoeffective (S-GE in Table 1), they have a low average value of Dst (−176 nT), high average value of CME speeds (761 $km\,s^{-1}$), and large average direction parameter (0.72). CMEs from the NW quadrant, on the other hand, are in equal portions strongly and moderately geoeffective (25%) with an average Dst of −125 nT. They have an even higher average value of CME speeds of 938 $km\,s^{-1}$, but lower average value of the direction parameter. CMEs from the eastern quadrants have higher minimum Dst values and lower speeds than those from the western quadrants and direction parameters

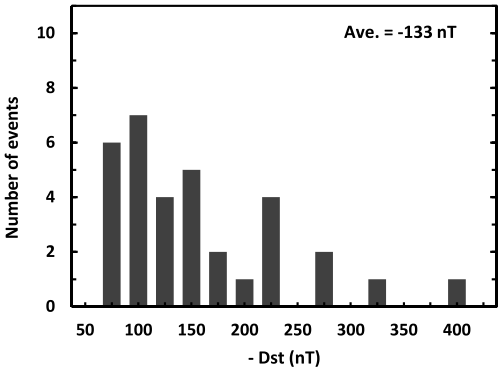

Figure 3 Distribution of the Dst indices associated with geoeffective disk-centre full-halo CMEs. The average minimum Dst value is given in the panel.

comparable to CMEs from the NW quadrant (Table 1). The large average direction parameter of the DC-FH-CMEs from the SW quadrant might explain the higher rate of strongly geoeffective CMEs compared to the three other quadrants.

The distributions of the Dst indices associated with geoeffective (Dst ≤ -50 nT) disk-centre full-halo CMEs during the studied period are presented in Figure 3. Thirty-three out of the 66 disk-centre full-halo CMEs were associated with 30 geomagnetic storms with Dst ≤ -50 nT. The range of the Dst minimum values was from -56 nT to -383 nT with an average of -133 nT. Thirteen of the 66 (20%) DC-FH-CMEs were associated with 13 moderate storms, while there were 20 (30%) DC-FH-CMEs associated with 17 strong storms. Twenty-six geomagnetic storms (87%) were associated with a single DC-FH-CME. These storms together with the relevant CME, associated shock, and ICME information are presented in Table 2. The average Dst minimum value of the storms associated with single DC-FH-CMEs was -122 nT. Four out of 30 storms (13%) were associated with multiple CMEs. These events are presented in Table 3. All these storms were complex and in all cases there was a fast CME launched from the Sun later than the other involved CMEs. The initial speeds and estimated arrival times of the CMEs indicated that the fast CME had overtaken the slower ones on their way to 1 AU. In these four cases, all involved DC-FH-CMEs were considered geoeffective. All CMEs causing a single complex storm were launched from the same active region and originated from close to disk centre, although not all of them fulfilled our criteria of a disk-centre full-halo CME. The average minimum Dst of these storms was -195 nT. This high average value of minimum Dst is in agreement with previous findings that the strongest geomagnetic storms are caused by complex interplanetary structures involving two or more CMEs (see Gonzalez *et al.*, 2011, and references therein). We also note that all four complex storms of Table 3 occurred in Solar Cycle 23.

The other half (33) of the disk-centre full-halo CMEs was nongeoeffective. Eight of the CMEs in this group (events 9, 12, 27, 30, 49, 55, 58, and 61 in Table 6) caused interplanetary shocks and ICMEs observed at Earth, but the minimum Dst values associated with these CMEs ranged only from -14 nT to -41 nT. For the rest 25 out of the 33 nongeoeffective DC-FH-CMEs no impact with Earth within the used ± 24-hour time window could be confirmed taking also into account in some cases the possibility of a high-speed solar wind stream as the cause of the weak (Dst > -50 nT) geomagnetic activity.

Table 2 Storms and ICMEs associated with single DC-FH-CMEs.

N[0][a]	CME (dd/mm/yy UT)	Velocity ($km\,s^{-1}$)	Disturbance[b] (dd/mm UT)	ICME[b] (dd/mm UT)	ICME[c] Type	V_{sw}[d] ($km\,s^{-1}$)	Storm (dd/mm UT)	Dst (nT)
1	06/01/97 15:10	523	10/01 01:04	10/01 04	MC	457	10/01 08	−78
6	15/10/98 10:04	262	18/10 19:52	19/10 04	MC	430	19/10 16	−112
7	04/11/98 07:54	523	07/11 08:15	07/11 22	LMC	535	07/11 17	−81
13	14/07/00 10:54	1674	15/07 14:37	15/07 19	MC	1089	16/07 01	−301
14	25/07/00 03:30	528	28/07 06:34	28/07 12	MC	481	29/07 12	−71
17	02/10/00 03:50	525	03/10 00:54	03/10 10	MC	460	04/10 21	−143
18	02/10/00 20:26	569	05/10 03:26	05/10 13	LMC	530	05/10 14	−182
19	03/11/00 18:26	291	06/11 09:48	06/11 17	MC	610	06/11 22	−159
21	24/11/00 15:30	1245	26/11 11:58	27/11 08	EJ	628	27/11 03	−80
22	18/12/00 11:50	510	22/12 19:25	23/12 00	EJ	328	23/12 05	−62
28	15/04/02 03:50	720	17/04 11:07	17/04 16	MC	611	18/04 08	−127
29	08/05/02 13:50	614	11/05 10:14	11/05 15	LMC	443	11/05 20	−110
32	14/08/03 20:06	378	17/08 14:21	18/08 01	MC	530	18/08 16	−148
33	29/10/03 20:54	2029	30/10 16:19	31/10 02	LMC	1700	30/10 23	−383
35	20/01/04 00:06	965	22/01 01:37	22/01 08	EJ	666	22/01 14	−130
38	08/12/04 20:26	611	11/12 13:40	12/12 22	LMC	468	13/12 03	−56
41	07/07/05 17:06	683	10/07 03:37	10/07 10	LMC	484	10/07 21	−92
42	13/09/05 20:00	1866	15/09 08:25	15/09 14	EJ	881	15/09 17	−80
44	03/04/10 10:33	668	05/04 08:26	05/04 12	MC	814	06/04 15	−81
50	14/06/12 14:12	987	16/06 20:19	16/06 23	MC	519	17/06 14	−71
51	12/07/12 16:48	885	14/07 18:09	15/07 06	MC	667	15/07 19	−127
54	02/09/12 04:00	538	04/09 22:45	05/09 06	MC	545	05/09 06	−68
60	16/02/14 10:00	634	19/02 03:48	19/02 12	MC	530	19/02 09	−116
63	10/09/14 18:00	1267	12/09 15:53	12/09 22	MC	730	13/09 00	−75
65	22/06/15 18:36	1209	24/06 14:00	25/06 10	EJ	731	25/06 16	−86
66	16/12/15 09:24	677	19/12 15:00	20/12 03	MC	497	20/12 23	−155

[a]Number of DC-FH-CME in Table 6.

[b]From the list of near-Earth interplanetary coronal mass ejections of Richardson and Cane (2010) or from the list of IP shocks of Gopalswamy *et al.* (2010a).

[c]MC = magnetic cloud, LMC = magnetic cloud like, EJ = ejecta.

[d]The maximum value of solar wind speed (see Section 5).

4. Geomagnetic Storm Strength and Properties of Disk-centre Full-halo Coronal Mass Ejections

The distributions of the CME linear sky-plane speeds and direction parameters of geoeffective and nongeoeffective disk-centre full-halo CMEs are presented in Figure 4. We define and determine the direction parameter (DP) of a CME following Moon *et al.* (2005) (see also, Kim *et al.*, 2008; Moon, Kim, and Cho, 2009). The direction parameter quantifies the symmetric characteristics of a CME seen in a coronagraph image and is defined as the maximum value of the ratio of the shorter distance of the CME front from the solar disk centre

Table 3 Storms and ICMEs associated with multiple CMEs with at least one DC-FH-CME involved.

N0[a]	CME (dd/mm/yy UT)	Velocity ($km\,s^{-1}$)	Disturbance[b] (dd/mm UT)	ICME[b] (dd/mm UT)	ICME[c] Type	V_{sw}[d] ($km\,s^{-1}$)	Storm (dd/mm UT)	Dst (nT)
	02/05/98 14:06[e]	938	04/05 02:15	04/05 06	EJ	833	04/05 10	−205
5	02/05/98 05:31[e]	542						
4	01/05/98 23:40[e]	585						
16	16/09/00 05:18[f]	1215	17/09 16:57	18/09 00	MC	840	17/09 21	−201
15	15/09/00 21:50[f]	257						
	15/09/00 15:26[f]	481						
	15/09/00 12:06[f]	633						
25	10/04/01 05:30[g]	2411	11/04 13:43	11/04 22	MC	732	12/04 00	−271
24	09/04/01 15:54[g]	1192						
40	15/01/05 23:06[h]	2861	17/01 07:15	17/01 13	EJ	798	18/01 09	−103
	15/01/05 06:39[h]	2049						

[a]Number of DC-FH-CME in Table 6.

[b]From the list of near-Earth interplanetary coronal mass ejections of Richardson and Cane (2010) or from the list of IP shocks of Gopalswamy *et al.* (2010a).

[c]MC = magnetic cloud, LMC = magnetic cloud like, EJ = ejecta.

[d]The maximum value of solar wind speed (see Section 5).

[e]All full-halo CMEs from active region 8210.

[f]Two full and two partial halo CMEs from active region 9165.

[g]Both from active region 9415.

[h]Both full-halo CMEs from active region 10720.

to the larger one when both are measured along the same line (see, *e.g.*, Figure 1 of Moon *et al.*, 2005).

The CME speed distribution peaks for geoeffective and nongeoeffective events at 600 $km\,s^{-1}$. The average values of the sky-plane speeds are 911 $km\,s^{-1}$ for geoeffective and 615 $km\,s^{-1}$ for nongeoeffective CMEs (Figure 4a). For all DC-FH-CMEs the average value of the sky-plane speed was 763 $km\,s^{-1}$. The average speed for the strongly geoeffective events was 964 $km\,s^{-1}$ and 829 $km\,s^{-1}$ for the moderately geoeffective events. The average speed for all DC-FH-CMEs in Solar Cycle 23 was 830 $km\,s^{-1}$, while in Solar Cycle 24 it was 637 $km\,s^{-1}$. We note that according to Gopalswamy, Yashiro, and Akiyama (2007) the average speed of disk halo CMEs during SC23 was 933 $km\,s^{-1}$, which is higher than the average speed of DC-FH-CMEs. The larger projection effects of DC-FH-CMEs may be the cause of this difference. The number of DC-FH-CMEs with high speeds ($\geq 600\,km\,s^{-1}$) was 33 out of 66 events (50%) of which 20 were geoeffective (geoeffectiveness rate of 61%) with an average minimum Dst of the associated storms of −139 nT. The number of events with low speeds ($< 600\,km\,s^{-1}$) was also 33 (50%) of which 13 were geoeffective (rate of 39%). The associated storms had the average minimum Dst of −126 nT.

The distributions of the direction parameters for geoeffective and nongeoeffective DC-FH-CMEs are presented in Figure 4b. The average values of the direction parameter for geoeffective and nongeoeffective events are 0.65 and 0.57, respectively, while for all DC-FH-CMEs it is 0.61. These values indicate that on average DC-FH-CMEs propagate toward the Earth fairly well coaligned with the Sun–Earth line. The number of DC-FH-CMEs with

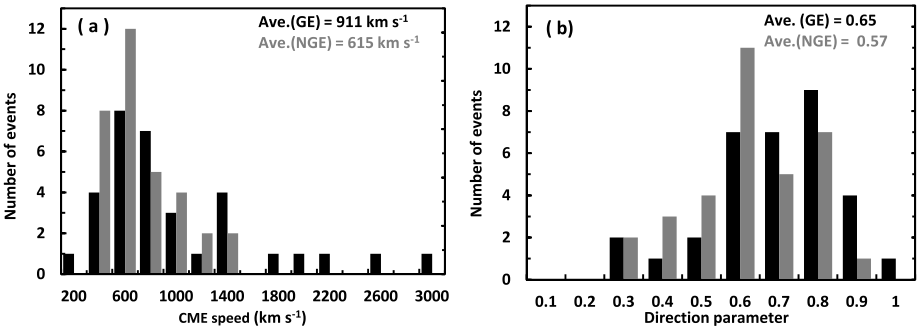

Figure 4 (a) Distributions of the CME sky-plane speeds and (b) direction parameters for geoeffective (black columns) and nongeoeffective (grey columns) disk-centre full-halo CMEs. The average values of the parameters for geoeffective (GE) and nongeoeffective (NGE) DC-FH-CMEs are given in the plots.

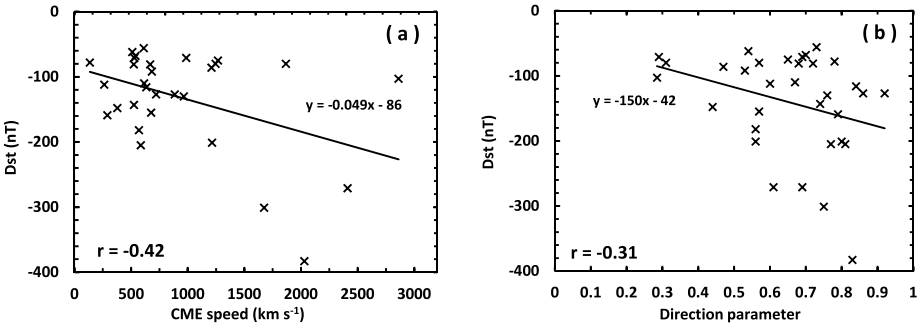

Figure 5 (a) Scatterplot between the Dst index and the CME sky-plane speed and (b) the direction parameter for geoeffective DC-FH-CMEs. The line is a linear fit to the data points. The correlation coefficients are given in the plots.

DP $\geq$ 0.4 is 58 out of 66 events (88%) of which 30 were geoeffective (geoeffectiveness rate of 52%) with an average value of minimum Dst of -137 nT. The number of events with DP $<$ 0.4 is eight (12%) of which three were geoeffective (rate of 38%) with an average value of minimum Dst of -85 nT. Seven out of eight DC-FH-CMEs associated with storms with Dst ≤ -200 nT had a direction parameter $\geq$ 0.6. The remaining one had DP $=$ 0.56 (see Figure 5b). These results are comparable to those of Kim *et al.* (2008).

We also studied the associations of the DC-FH-CMEs with solar soft X-ray flares. The number of DC-FH-CMEs associated with solar soft X-ray flares was 60 (91%). The flares had a wide distribution from class A1.1 to class X10.0 with an average of class M8.4. Of the 33 geoeffective DC-FH-CMEs, 31 were associated with X-ray flares, while 29 out of 33 nongeoeffective DC-FH-CMEs were also associated with flares. The average solar soft X-ray flux of geoeffective DC-FH-CMEs corresponded to class X1.0, while for nongeoeffective CMEs it was M6.3. From the total of 60 DC-FH-CMEs for which the flare association was found, 37 (62%) were associated with solar flare classes $\geq$ M1.0. From these, 17 were geoeffective (geoeffectiveness rate of 46%) with average minimum Dst of the associated storms of -149 nT. The rest 23 events (38%) out of 60 were associated with $<$ M1.0 flares of which 14 were geoeffective (rate of 61%) with average value of minimum Dst of -122 nT.

Figure 5 shows the dependence of the strength of the geomagnetic storms associated with the geoeffective DC-FH-CMEs on the CME sky-plane speed and direction parameter. For the three storms associated with two almost simultaneous DC-FH-CMEs, the speed of the faster DC-FH-CME was used. There is a relatively weak negative correlation between the Dst index and the CME sky-plane speed with a correlation coefficient of -0.42 (Figure 5a). The Student t-test, however, gives a significance level of 0.99 for the correlation ($P = 0.010$). Similar correlations have been reported by Srivastava and Venkatakrishnan (2004), Kim *et al.* (2005), Gopalswamy (2009), Vasanth and Umapathy (2013), and Shanmugaraju *et al.* (2015). We also examined the correlation between Dst and the space speed of the DC-FH-CMEs, as given in the SOHO/LASCO halo CME catalogue. We found practically the same correlation ($r = -0.41$) as between Dst and the sky-plane speed of the CMEs. Figure 5b shows a weak negative correlation between the Dst and the direction parameter with a correlation coefficient of -0.31 ($P = 0.048$). Thus, although DC-FH-CMEs with a large value of the direction parameter are well associated with the strongest storms (Dst ≤ -200 nT), the overall storm strength cannot be well explained by the direction parameter alone.

5. Solar Wind Conditions and Geomagnetic Storms

We use OMNI data[4] to examine the solar wind conditions at the time of the geomagnetic storms (Dst ≤ -50 nT) associated with geoeffective DC-FH-CMEs. The solar wind parameters measured at 1 AU which we investigated include the total magnetic field strength, B_t, the southward component of the magnetic field, $B_s = -B_z$ in geocentric solar magnetospheric (GSM) coordinates, the solar wind speed, V_{sw}, and the y-component of the solar wind electric field, $E_y \sim -B_z V_{sw}$. For all of these quantities including the Dst index we used 1-hour averages. Similar to Kim *et al.* (2014), we associated these parameters to geoeffective disk-centre full-halo CMEs by using a time window starting 24 hours before the expected CME arrival time and ending at the observed Dst minimum time. The CME arrival time prediction is based on the drag-based model (Vršnak *et al.*, 2013). The maximum values of the solar wind parameters within this time window are selected to represent the characteristics of the interplanetary counterparts of the DC-FH-CMEs. Figure 3 shows the distribution of the Dst minimum values measured during the passage of the IP disturbances related to the DC-FH-CMEs. The average minimum value of the Dst index for geomagnetic storms associated with geoeffective DC-FH-CMEs (30 storms) was -133 nT (see Section 3). The average maximum values of B_t, B_s, V_{sw}, and E_y related to those 30 storms were 23.8 nT, 15.9 nT, 656 km s^{-1}, and 11.3 mV m^{-1}, respectively.

Figure 6 shows a very strong negative correlation between the Dst index and B_t, B_s, and E_y with correlation coefficients of $r = -0.76$, -0.77, and -0.87, respectively. There is also a good negative correlation with V_{sw} with a correlation coefficient of $r = -0.73$. All these correlations are significant at a $> 99.9\%$ confidence level. The strong correlation between Dst and B_s is of course expected. As well, the strong correlation between the product of the solar wind speed and the southward component of the IP magnetic field (*i.e.* E_y) has been reported, *e.g.*, by Gopalswamy *et al.* (2015a) when studying the geoeffectiveness of magnetic clouds.

To investigate relations between the initial CME speed and the solar wind conditions at 1 AU, we examined the correlations between the CME sky-plane speed and the southward

[4] http://omniweb.gsfc.nasa.gov.

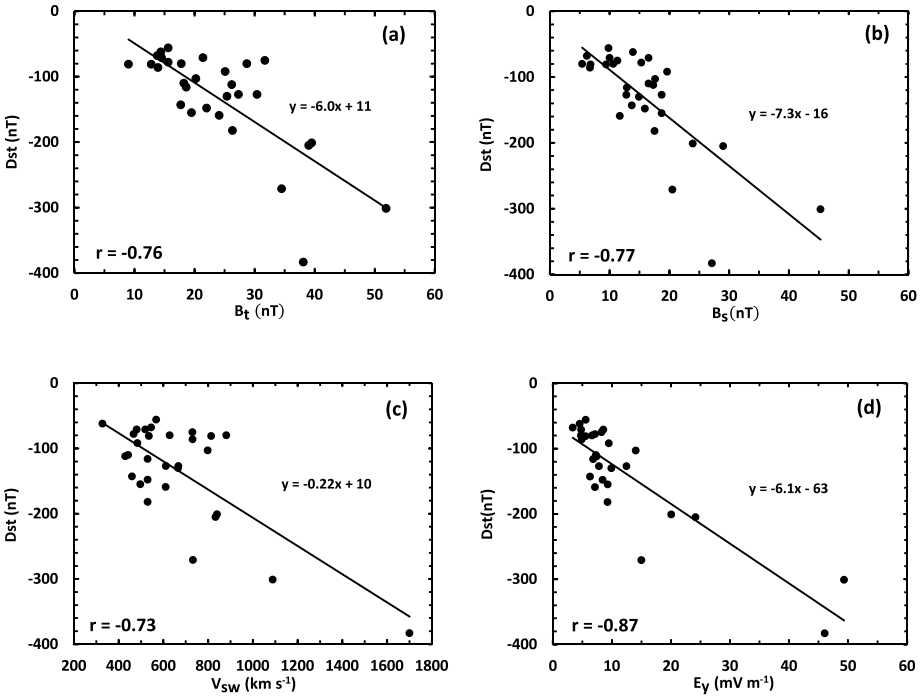

Figure 6 Scatterplots between the Dst index and the solar wind parameters (B_t, B_s, V_{sw}, and E_y). The lines are linear fits to the data points. The correlation coefficients between the Dst index and each of the solar wind parameters are shown in the plots.

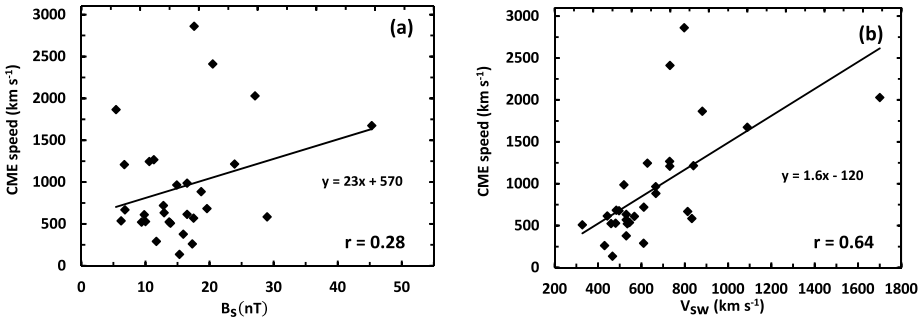

Figure 7 (a) Scatterplots between the initial CME sky-plane speed and the southward component of the IP magnetic field and (b) the solar wind speed at 1 AU. The lines are linear fits to the data points. The correlation coefficients are shown in the plots.

component of the IP magnetic field and the solar wind speed measured at 1 AU for all geomagnetic storms associated with geoeffective DC-FH-CMEs. For the storms associated with two almost simultaneous DC-FH-CMEs, the speed of the faster DC-FH-CME was used. Figure 7a shows only a weak correlation between B_s and the CME speed with the correlation coefficient of 0.28, which is not significant ($P = 0.07$). As expected, there is a much better correlation between the initial CME speed and the solar wind speed ($r = 0.64$,

Table 4 Solar cycle variations of the number of the disk-centre full-halo CMEs and their geoeffectiveness. The upper half of the table is for Solar Cycle 23 and the lower half for Cycle 24.

Phase	S-GE[a]	M-GE[b]	Dst ≤ -50 nT	Average Dst	Nongeoeffective	Total
SC23						
Rise	3 (38%)	2 (25%)	5 (63%)	−119 nT	3 (37%)	8
Maximum	10 (48%)	3 (14%)	13 (62%)	−155 nT	8 (38%)	21
Decay	4 (29%)	3 (21%)	7 (50%)	−142 nT	7 (50%)	14
Total	17 (39%)	8 (19%)	25 (58%)	−144 nT	18 (42%)	43
SC24						
Rise	0 (0%)	1 (25%)	1 (25%)	−81 nT	3 (75%)	4
Maximum	2 (12%)	3 (17%)	5 (29%)	−91 nT	12 (71%)	17
Decay[c]	1 (50%)	1 (50%)	2 (100%)	−121 nT	0 (0%)	2
Total	3 (13%)	5 (22%)	8 (35%)	−97 nT	15 (65%)	23

[a]Strongly geoeffective.

[b]Moderately geoeffective.

[c]Till the end of December 2015.

$P < 0.001$), because the measured solar wind speed is that of the interplanetary counterpart of the DC-FH-CME causing the geomagnetic storm.

6. Properties of DC-FH-CMEs and the Associated Geomagnetic Storms in Solar Cycles 23 and 24

To study the solar cycle dependence of the number and geoeffectiveness of disk-centre full-halo CMEs, we divided our study period into rise, maximum, and decay phases of the solar cycles. For Solar Cycle 23 we used the periods May 1996 – December 1998, January 1999 – May 2002, and June 2002 – November 2008 for the rise, maximum, and decay phases, respectively (Gopalswamy *et al.*, 2015a). For Solar Cycle 24 the corresponding periods were December 2008 – August 2011, September 2011 – December 2014, and January 2015 – December 2015 with the decay phase still continuing at the end of 2015. Thus we take the rise and maximum phases of Solar Cycles 23 and 24 of comparable lengths. Table 4 shows the numbers and percentage fractions of geoeffective disk-centre full-halo CMEs from the total numbers of DC-FH-CMEs during the rise, maximum, and decay phases of SC23 and SC24. Statistics for strongly geoeffective (S-GE, column 2), moderately geoeffective (M-GE, column 3), and for all geoeffective DC-FH-CMEs (Dst ≤ -50 nT, column 4) are shown separately in Table 4. The largest number of DC-FH-CMEs occurs at the maximum phases of SC23 (21) and SC24 (17). During the maximum phase of SC23 the geoeffectiveness rate (62%) is much higher and the average value of Dst of the associated storms (-155 nT) much lower than during the corresponding phase of SC24 (29% and -91 nT, respectively). In the rise phase of SC23 there were several DC-FH-CMEs (eight) and they had a high rate of geoeffectiveness (63%; five out of eight). In the rise phase of SC24 there were only four events, one of them moderately geoeffective with Dst of -81 nT and the other events nongeoeffective. During SC23, the total number of strongly geoeffective events was higher than that of the moderately geoeffective events, while during SC24 it was lower, which reflects the effect of the strength of the activity cycle.

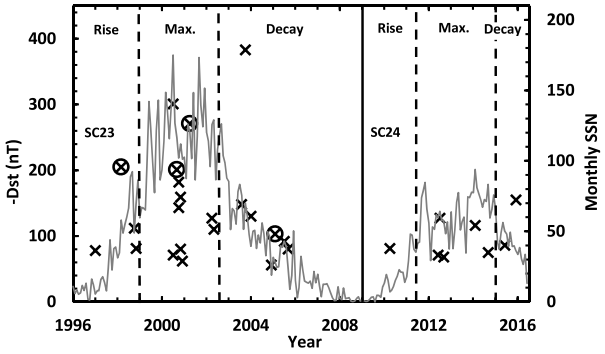

Figure 8 Time dependence of the strength of geomagnetic storms caused by the disk-centre full-halo CMEs. The crosses represent the storms with Dst minimum values ≤ -50 nT. The crosses surrounded by circles represent storms associated with multiple CMEs. For comparison, the monthly average sunspot number is also shown. The vertical line separates Solar Cycles 23 and 24 and the dashed lines separate various phases of the cycles.

In general, the geoeffectiveness rate of DC-FH-CMEs was higher (58%) and the average values of minimum Dst lower (-144 nT) in SC23 than in SC24 (35% and -97 nT, respectively). Table 4 shows that the number of disk-centre full-halo CMEs in Solar Cycle 23 was almost twice that in Cycle 24 (till the end of December 2015). Gopalswamy *et al.* (2015b) reported that halo CMEs during the first 73 months of Cycle 24 were more abundant than during the corresponding epoch of Cycle 23. During the first 85 months of the cycles the situation was still the same. However, the numbers of front-side halo CMEs, for which the source locations are given in the halo CME catalogue, are comparable during the first 85 months of the two cycles and even higher in SC23 (166 in SC23 and 147 in SC24). The finding of Gopalswamy *et al.* (2015b) that the longitude distribution of halo CMEs in Cycle 24 was much flatter than in Cycle 23 may explain the significantly lower number of DC-FH-CMEs (within $\pm 10^\circ$ from the central meridian) in Cycle 24 compared to Cycle 23. The lower geoeffectiveness of the DC-FH-CMEs during SC24 is explained by the lower mean speed of the CMEs and by the reduced southward magnetic field component of the IP magnetic structures encountering Earth during Cycle 24 (Gopalswamy *et al.*, 2015a).

Figure 8 shows the Dst indices of the 30 geomagnetic storms associated with the geoeffective disk-centre full-halo CMEs as a function of time. The number and strength of the storms loosely follow the monthly average sunspot number. The geomagnetic storms associated with multiple CMEs are presented in Figure 8 with crosses surrounded by circles. Most of the storms with Dst ≤ -100 nT occurred at or close to the maximum phases of SC23 and SC24. All the complex storms associated with multiple CMEs occurred in SC23, three of the four close to the cycle maximum phase. During the decay phase of SC23 most of the events were only moderately geoeffective. This is in accordance with the trend of stronger geomagnetic storms to occur in the maximum phase of the solar cycle (*e.g.* Kilpua *et al.*, 2015). From the poor statistics of SC24 in our data this trend is less evident.

Considering epochs of equal lengths during Solar Cycles 23 and 24, we examined the properties of DC-FH-CMEs, associated solar wind parameters, and geomagnetic storms during the first 85 months of both cycles. For Cycle 23 this means the period from May 1996 to May 2003 and for Cycle 24 the period from December 2008 to December 2015. The sunspot numbers averaged over these periods were 79.98 in Cycle 23 and 42.76 in Cycle 24. Thus, the average sunspot number declined by 46.5%. Table 5 shows the average values of the

Table 5 Properties of disk-centre full-halo CMEs, the associated solar wind parameters at 1 AU, and geomagnetic storms during the first 85 months of Solar Cycles 23 and 24.

Parameter	SC23	SC24	Change
All DC-FH-CMEs			
N^0 of events	31	23	−26%
Average CME speed ($km\,s^{-1}$)	732	637	−13%
Average DP	0.66	0.58	−12%
Geoeffective DC-FH-CMEs			
N^0 of geoeffective events	18	8	−56%
Geoeffectiveness rate	58%	35%	−40%
Average CME speed ($km\,s^{-1}$)	767	858	+12%
Average DP	0.69	0.66	−4%
Average B_t (nT)	26.3	19.4	−26%
Average B_s (nT)	17.8	12.2	−31%
Average V_{sw} ($km\,s^{-1}$)	601	629	+5%
Average E_y ($mV\,m^{-1}$)	12.1	7.4	−39%
Average |Dst| (nT)	146	97	−34%

sky-plane speeds and direction parameters of all DC-FH-CMEs together with the average values of the CME and solar wind parameters associated with geoeffective DC-FH-CMEs during epochs of equal lengths of Solar Cycles 23 and 24. The last column of Table 5 shows the change from SC23 to SC24 for each parameter. In general, all parameter values are reduced; notice that for Dst we refer to its absolute value. The CME and corresponding solar wind speed of geoeffective DC-FH-CMEs were exceptions with slightly higher values in SC24 compared to SC23. The number of all DC-FH-CMEs was reduced by 26%. Reductions in the initial CME speed (13%) and direction parameter (12%) were small. There was a large reduction in the number of geoeffective DC-FH-CMEs (56%), which is significantly larger than the decline in the number of all DC-FH-CMEs (26%). The geoeffectiveness rate was also significantly reduced, while there was only a very small change in the direction parameter. Changes in the solar wind parameters B_t (−26%), B_s (−31%), and E_y (−39%) were also large. The changes in the geoeffectiveness rate of DC-FH-CMEs (40%) and in the average Dst of geoeffective DC-FH-CMEs (34%) from SC23 to SC24 are consequences of the lower B_s and E_y of the disturbances encountering Earth during Solar Cycle 24.

7. Summary and Conclusions

We have investigated the geoeffectiveness of front-side full-halo CMEs launched from close to the central meridian of the Sun (DC-FH-CMEs) from 1996 till the end of 2015. These CMEs are usually well directed towards the Earth and can be considered as plausible candidates for sources of geomagnetic storms. We have identified 66 DC-FH-CMEs, which originated from source locations between solar longitudes E10 and W10 and latitudes N20 and S20. We found that 33 (50%) out of total 66 DC-FH-CMEs caused 30 geomagnetic storms with Dst ≤ -50 nT. Of the 30 geomagnetic storms, 26 were associated with single disk-centre full-halo CMEs, while four storms were associated, in addition to at least

one disk-centre full-halo CME, also with other halo or wide CMEs from the same active region. Thirteen (20%) DC-FH-CMEs were associated with 13 moderate geomagnetic storms (-100 nT $<$ Dst ≤ -50 nT) and 20 (30%) were associated with 17 strong storms (Dst ≤ -100 nT). The average values of the Dst indices were -133 nT for all geomagnetic storms, -75 nT for moderate, and -177 nT for strong storms. We also found that geoeffective CMEs originated more frequently from the south–west and north–west quadrants than from south–east and north–east quadrants of the investigated longitude–latitude range. Half of the DC-FH-CMEs associated with strong storms originated from the SW quadrant with a total of three quarters from the western quadrants, while slightly more than half of the moderately geoeffective CMEs originated from the eastern quadrants.

From the distributions of the initial sky-plane speeds of the DC-FH-CMEs, we obtained the average speed of 911 km s^{-1} for the geoeffective CMEs and 615 km s^{-1} for the non-geoeffective events. For moderately and strongly geoeffective CMEs the average speeds were 829 km s^{-1} and 964 km s^{-1}, respectively. From the 66 DC-FH-CMEs 58 (88%) had a direction parameter ≥ 0.4 and 30 (52%) of these were geoeffective. Only eight (12%) DC-FH-CMEs had a direction parameter < 0.4 and three of these were geoeffective (38%). Seven out of eight DC-FH-CMEs associated with storms with Dst ≤ -200 nT had a direction parameter ≥ 0.6. Both geoeffective and nongeoeffective DC-FH-CMEs were strongly associated with large solar soft X-ray flares. The average X-ray flux of geoeffective CMEs corresponded to class X1.0, while for nongeoeffective CMEs it was M6.3.

When studying the dependence of the storm strength on the initial CME sky-plane speed and on the direction parameter, we obtained the linear correlation coefficients of $r = -0.42$ and $r = -0.31$ between the minimum Dst and the CME speed and Dst and the direction parameter, respectively. Thus, neither of these two DC-FH-CME parameters can alone be used to satisfactorily explain the storm strength.

From the solar wind parameters associated with the disk-centre full-halo CMEs the total magnetic field strength, the southward component of the magnetic field, and the y-component of the solar wind electric field best correlated with the storm strength. The linear correlation coefficients for these quantities were -0.76, -0.77, and -0.87, respectively. A good negative correlation was also found between Dst and the solar wind speed at 1 AU ($r = -0.73$). We also examined the correlation between the southward component of the magnetic field and the solar wind speed with the CME sky-plane speed. There was a weak, insignificant correlation between B_s and CME speed ($r = 0.28$), while the correlation was strong between E_y and CME speed ($r = 0.70$).

We investigated the dependences of the properties of DC-FH-CMEs and the associated geomagnetic storms on different phases of the solar cycles and the differences between Solar Cycles 23 and 24. In the rise phase of SC23, five out of eight DC-FH-CMEs were geoeffective. In the corresponding phase of SC24, only four DC-FH-CMEs were observed, one moderately geoeffective and the rest nongeoeffective. The largest number of DC-FH-CMEs occurred at the maximum phases of both SC23 (21) and SC24 (17). Most of the storms with Dst ≤ -100 nT occurred at or close to the maximum phases of SC23 and SC24. All the complex storms associated with multiple CMEs occurred in SC23, three of the four close to the cycle maximum phase.

The average values of minimum Dst in all phases of SC23 were lower than in SC24 during the corresponding phases. In SC23, strongly geoeffective DC-FH-CMEs were more abundant than moderately geoeffective, while in SC24 it was *vice versa*. In general, the geoeffectiveness rate of DC-FH-CMEs was higher (58%) and the average values of minimum Dst lower (-144 nT) in SC23 than in SC24 (35% and -97 nT, respectively).

The number of disk-centre full-halo CMEs during the first 85 months of Solar Cycle 23 was significantly higher than during the corresponding epoch of Solar Cycle 24 (31 *vs.* 23).

In particular, the number of geoeffective DC-FH-CMEs was reduced by 56% from SC23 to SC24. The changes in the geoeffectiveness rate of DC-FH-CMEs (40%) and in the average minimum Dst of geoeffective DC-FH-CMEs (34%) from SC23 to SC24 are believed to be consequences of the reduced magnitudes of the southward magnetic field component and the y-component of the solar wind electric field of the interplanetary counterparts of disk-centre full-halo CMEs during Solar Cycle 24.

Acknowledgements The authors gratefully acknowledge the various online data centres of NOAA and NASA for providing the data. We also express our thanks to the world data centre in Kyoto for minimum Dst values and NSSDCs OMNI web services for interplanetary magnetic field data. The CME catalogue we have used is generated and maintained by the Center for Solar Physics and Space Weather, The Catholic University of America in cooperation with the Naval Research Laboratory and NASA. D.A. acknowledges support by the Ministry of Higher Education and Scientific Research of Iraq under grant 4552/2013.

Disclosure of Potential Conflict of Interest The authors declare that they have no conflict of interest.

Appendix

Table 6 Dates and properties of disk-centre full-halo CMEs from May 1996 to December 2015

N^0	Date[a] dd/mm/yy	Time[b] hh:mm	V[c] km s^{-1}	DP[d]	Flare[e] class	Solar location	B0 angle degree	AR[f] N^0
1	06/01/97	15:10	136	0.78	A1.1	S18E06	−3.7	···
2	21/10/97	18:03	523	0.60	C3.3	N16E07	+5.3	8097
3	27/02/98	20:07	422	0.52	B1.5	S24E07	−7.2	···
4	01/05/98	23:40	585	0.77	M1.2	S18W05	−4.1	8210
5	02/05/98	05:31	542	0.81	C5.4	S20W07	−4.1	8210
6	15/10/98	10:04	262	0.60	···	N22W01	+5.9	···
7	04/11/98	07:54	523	0.68	C1.6	N17W01	+4.1	8375
8	05/11/98	02:02	380	0.84	C7.1	N19W10	+4.0	8375
9	29/06/99	19:54	560	0.72	M1.6	S14E01	+2.7	8603
10	30/06/99	11:54	406	0.80	M1.9	S15E00	+2.8	8603
11	10/04/00	00:30	409	0.75	M3.1	S14W01	−6.0	8948
12	07/07/00	10:26	453	0.56	···	N04E00	+3.6	···
13	14/07/00	10:54	1674	0.75	X5.7	N22W07	+4.3	9077
14	25/07/00	03:30	528	0.69	M8.0	N06W08	+5.3	9097
15	15/09/00	21:50	257	0.56	C7.4	N14E02	+7.2	9165
16	16/09/00	05:18	1215	0.80	M5.9	N14W07	+7.2	9165
17	02/10/00	03:50	525	0.74	C4.1	S09E07	+6.7	9176
18	02/10/00	20:26	569	0.56	C8.4	S09E00	+6.7	9176
19	03/11/00	18:26	291	0.79	C3.2	N02W02	+4.1	9213
20	24/11/00	05:30	1289	0.58	X2.0	N20W05	+1.7	9236
21	24/11/00	15:30	1245	0.57	X2.3	N22W07	+1.7	9236
22	18/12/00	11:50	510	0.54	C7.0	N15E01	−1.4	9269
23	19/03/01	05:26	389	0.79	···	S20W00	−7.1	···
24	09/04/01	15:54	1192	0.69	M7.9	S21W04	−6.0	9415
25	10/04/01	05:30	2411	0.61	X2.3	S23W09	−6.0	9415
26	13/12/01	14:54	864	0.42	X6.2	N16E09	−0.7	9733
27	15/03/02	23:06	957	0.61	M2.2	S08W03	−7.2	9866
28	15/04/02	03:50	720	0.86	M1.2	S15W01	−5.6	9906

Table 6 (*Continued.*)

N^0	Date[a] dd/mm/yy	Time[b] hh:mm	V[c] km s^{-1}	DP[d]	Flare[e] class	Solar location	B0 angle degree	AR[f] N^0
29	08/05/02	13:50	614	0.67	C4.2	S12W07	−3.4	9934
30	15/07/02	20:30	1151	0.35	X3.0	N19W01	+4.4	10030
31	19/12/02	22:06	1092	0.55	M2.7	N15W09	−1.5	10229
32	14/08/03	20:06	378	0.44	...	S10E02	+6.6	...
33	29/10/03	20:54	2029	0.83	X10.0	S15W02	+4.6	10486
34	20/11/03	08:06	669	0.49	M9.6	N01W08	+2.3	10501
35	20/01/04	00:06	965	0.76	C5.5	S13W09	−5.0	10540
36	06/11/04	01:31	818	0.49	M5.9	N09E05	+3.8	10696
37	03/12/04	00:26	1216	0.50	M1.5	N08W02	+0.6	10708
38	08/12/04	20:26	611	0.73	C2.5	N05W03	−0.2	10709
39	14/02/05	17:06	358	0.66	M1.0	S06E02	−4.5	10720
40	15/01/05	23:06	2861	0.29	X2.6	N15W05	−4.6	10720
41	07/07/05	17:06	683	0.53	M4.9	N09E03	+3.6	10786
42	13/09/05	20:00	1866	0.31	X1.5	S09E10	+7.2	10808
43	30/04/06	09:54	544	0.58	C1.8	S10E08	−4.2	10876
44	03/04/10	10:33	668	0.72	B7.4	S25E00	−6.4	...
45	23/05/10	18:06	258	0.55	B1.4	N16W10	−1.7	...
46	14/02/11	18:24	326	0.70	M2.23	S20W04	−6.8	11158
47	21/06/11	03:16	719	0.63	C7.7	N16W08	+1.7	11236
48	06/09/11	02:24	782	0.36	M5.3	N14W07	+7.2	11283
49	12/05/12	00:00	805	0.30	...	S12E08	−3.0	...
50	14/06/12	14:12	987	0.29	M1.9	S17E06	+1.0	11504
51	12/07/12	16:48	885	0.92	X1.4	S15W01	+4.1	11520
52	13/08/12	13:25	435	0.29	C2.8	N22W03	+6.6	11543
53	14/08/12	01:25	634	0.33	C3.5	N23W08	+6.6	11543
54	02/09/12	04:00	538	0.70	C2.9	N03W05	+7.2	11560
55	21/11/12	16:00	529	0.63	M3.5	N05E05	+2.0	11618
56	22/10/13	21:48	459	0.72	M4.2	N04W01	+5.2	11875
57	24/10/13	01:25	399	0.56	M9.3	S10E08	+5.1	...
58	12/02/14	06:00	373	0.75	M3.7	S12W02	−6.7	11974
59	12/02/14	16:36	533	0.61	M2.1	S11W03	−6.7	11974
60	16/02/14	10:00	634	0.84	M1.1	S11E01	−6.9	11977
61	15/08/14	18:12	342	0.52	...	S10W05	+6.8	...
62	22/08/14	11:36	604	0.60	C2.2	N12E01	+6.9	...
63	10/09/14	18:00	1267	0.65	X1.6	N14E02	+7.3	12158
64	17/12/14	05:00	595	0.52	M8.7	S20E09	−1.2	12242
65	22/06/15	18:36	1209	0.47	M6.5	N12W08	+1.7	12371
66	16/12/15	09:24	677	0.57	C6.6	S13W04	−1.0	12468

[a]Date of the CME launch.

[b]Time (UT) first appearance of the CME in LASCO/C2.

[c]CME linear sky-plane speed.

[d]CME direction parameter.

[e]Ellipsis means that the flare class is not known.

[f]Active region number. Ellipsis means that the active region is not known.

References

Brueckner, G.E., Howard, R.A., Koomen, M.J., Korendyke, C.M., Michels, D.J., Moses, J.D., Socker, D.G., Dere, K.P., Lamy, P.L., Llebaria, A., Bout, M.V., Schwenn, R., Simnett, G.M., Bedford, D.K., Eyles, C.J.: 1995, The Large Angle Spectroscopic Coronagraph (LASCO). *Solar Phys.* **162**, 357. DOI. ADS.

Cane, H.V., Richardson, I.G., St. Cyr, O.C.: 2000, Coronal mass ejections, interplanetary ejecta and geomagnetic storms. *Geophys. Res. Lett.* **27**, 3591. DOI. ADS.

Dumbović, M., Devos, A., Vršnak, B., Sudar, D., Rodriguez, L., Ruždjak, D., Leer, K., Vennerstrøm, S., Veronig, A.: 2015, Geoeffectiveness of coronal mass ejections in the SOHO era. *Solar Phys.* **290**, 579. DOI. ADS.

Gonzalez, W.D., Joselyn, J.A., Kamide, Y., Kroehl, H.W., Rostoker, G., Tsurutani, B.T., Vasyliunas, V.M.: 1994, What is a geomagnetic storm? *J. Geophys. Res.* **99**, 5771. DOI. ADS.

Gonzalez, W.D., Echer, E., Tsurutani, B.T., Clúa de Gonzalez, A.L., Dal Lago, A.: 2011, Interplanetary origin of intense, superintense and extreme geomagnetic storms. *Space Sci. Rev.* **158**, 69. DOI. ADS.

Gopalswamy, N.: 2009, The CME link to geomagnetic storms. In: *IAU Symp.* **264**, 326. DOI.

Gopalswamy, N., Yashiro, S., Akiyama, S.: 2007, Geoeffectiveness of halo coronal mass ejections. *J. Geophys. Res.* **112**(A6). DOI.

Gopalswamy, N., Xie, H., Mäkelä, P., Akiyama, S., Yashiro, S., Kaiser, M., Howard, R., Bougeret, J.-L.: 2010a, Interplanetary shocks lacking type II radio bursts. *Astrophys. J.* **710**(2), 1111. DOI.

Gopalswamy, N., Yashiro, S., Michalek, G., Xie, H., Mäkelä, P., Vourlidas, A., Howard, R.A.: 2010b, A catalog of halo coronal mass ejections from SOHO. *Sun Geosph.* **5**, 7. ADS.

Gopalswamy, N., Yashiro, S., Xie, H., Akiyama, S., Mäkelä, P.: 2015a, Properties and geoeffectiveness of magnetic clouds during solar cycles 23 and 24. *J. Geophys. Res.* **120**(11), 9221. DOI.

Gopalswamy, N., Xie, H., Akiyama, S., Mäkelä, P., Yashiro, S., Michalek, G.: 2015b, The peculiar behavior of halo coronal mass ejections in solar cycle 24. *Astrophys. J. Lett.* **804**, L23. DOI. ADS.

Gosling, J.T., McComas, D.J., Phillips, J.L., Bame, S.J.: 1991, Geomagnetic activity associated with Earth passage of interplanetary shock disturbances and coronal mass ejections. *J. Geophys. Res.* **96**, 7831. DOI. ADS.

Kilpua, E.K.J., Olspert, N., Grigorievskiy, A., Käpylä, M.J., Tanskanen, E.I., Miyahara, H., Kataoka, R., Pelt, J., Liu, Y.D.: 2015, Statistical study of strong and extreme geomagnetic disturbances and solar cycle characteristics. *Astrophys. J.* **806**, 272. DOI. ADS.

Kim, R.-S., Cho, K.-S., Moon, Y.-J., Kim, Y.-H., Yi, Y., Dryer, M., Bong, S.-C., Park, Y.-D.: 2005, Forecast evaluation of the coronal mass ejection (CME) geoeffectiveness using halo CMEs from 1997 to 2003. *J. Geophys. Res.* **110**(A9), A11104. DOI. ADS.

Kim, R.-S., Cho, K.-S., Kim, K.-H., Park, Y.-D., Moon, Y.-J., Yi, Y., Lee, J., Wang, H., Song, H., Dryer, M.: 2008, CME earthward direction as an important geoeffectiveness indicator. *Astrophys. J.* **677**(2), 1378. DOI.

Kim, R.-S., Moon, Y.-J., Gopalswamy, N., Park, Y.-D., Kim, Y.-H.: 2014, Two-step forecast of geomagnetic storm using coronal mass ejection and solar wind condition. *Space Weather* **12**(4), 246. DOI.

Lee, J.-O., Moon, Y.-J., Lee, K.-S., Kim, R.-S.: 2014, Dependence of geomagnetic storms on their associated halo CME parameters. *Solar Phys.* **289**, 2233. DOI. ADS.

Lindsay, G.M., Russell, C.T., Luhmann, J.G.: 1995, Coronal mass ejection and stream interaction region characteristics and their potential geomagnetic effectiveness. *J. Geophys. Res.* **100**, 16999. DOI. ADS.

Loewe, C., Prölss, G.: 1997, Classification and mean behavior of magnetic storms. *J. Geophys. Res.* **102**(A7), 14209. DOI.

Mayaud, P.N.: 1980, *Derivation, Meaning, and Use of Geomagnetic Indices*. *AGU Geophys. Monograph Ser.* **22**. DOI. ADS.

Michalek, G.: 2006, An asymmetric cone model for halo coronal mass ejections. *Solar Phys.* **237**, 101. DOI. ADS.

Michałek, G., Gopalswamy, N., Yashiro, S.: 2003, A new method for estimating widths, velocities, and source location of halo coronal mass ejections. *Astrophys. J.* **584**, 472. DOI. ADS.

Michalek, G., Gopalswamy, N., Yashiro, S.: 2007, Prediction of space weather using an asymmetric cone model for halo CMEs. *Solar Phys.* **246**, 399. DOI. ADS.

Michalek, G., Gopalswamy, N., Lara, A., Yashiro, S.: 2006, Properties and geoeffectiveness of halo coronal mass ejections. *Space Weather* **4**, S10003. DOI. ADS.

Moon, Y.-J., Kim, R.-S., Cho, K.-S.: 2009, Geometrical implication of the CME earthward direction parameter and its comparison with cone model parameters. *J. Korean Astron. Soc.* **42**, 27. DOI.

Moon, Y.-J., Cho, K.-S., Dryer, M., Kim, Y.-H., Bong, S.-c., Chae, J., Park, Y.: 2005, New geoeffective parameters of very fast halo coronal mass ejections. *Astrophys. J.* **624**(1), 414. DOI.

Richardson, I., Cane, H.: 2010, Near-earth interplanetary coronal mass ejections during solar cycle 23 (1996 – 2009): catalog and summary of properties. *Solar Phys.* **264**(1), 189. DOI.

Richardson, I.G., Cane, H.V.: 2012, Solar wind drivers of geomagnetic storms during more than four solar cycles. *J. Space Weather Space Clim.* **2**(27), A01. DOI. ADS.

Shanmugaraju, A., Vršnak, B.: 2014, Transit time of coronal mass ejections under different ambient solar wind conditions. *Solar Phys.* **289**(1), 339. DOI.

Shanmugaraju, A., Ibrahim, M.S., Moon, Y.-J., Rahman, A.M., Umapathy, S.: 2015, Empirical relationship between CME parameters and geo-effectiveness of halo CMEs in the rising phase of solar cycle 24 (2011 – 2013). *Solar Phys.* **290**(5), 1417. DOI.

Srivastava, N., Venkatakrishnan, P.: 2004, Solar and interplanetary sources of major geomagnetic storms during 1996 – 2002. *J. Geophys. Res.* **109**(A18), A10103. DOI. ADS.

Tsurutani, B.T., Gonzalez, W.D.: 1997, *The Interplanetary Causes of Magnetic Storms: A Review*. *AGU Geophys. Monograph. Ser.* **98**, 77. DOI. ADS.

Vasanth, V., Umapathy, S.: 2013, A statistical study on DH CMEs and its geoeffectiveness. *ISRN Astron. Astrophys.* **2013**, 129426. DOI.

Vasanth, V., Chen, Y., Kong, X., Wang, B.: 2015, Investigation of the geoeffectiveness of CMEs associated with ip type II radio bursts. *Solar Phys.* **290**(6), 1815. DOI.

Vršnak, B., Žic, T., Vrbanec, D., Temmer, M., Rollett, T., Möstl, C., Veronig, A., Čalogović, J., Dumbović, M., Lulić, S., *et al.*: 2013, Propagation of interplanetary coronal mass ejections: the drag-based model. *Solar Phys.* **285**(1-2), 295. DOI.

Wang, Y.M., Ye, P.Z., Wang, S., Zhou, G.P., Wang, J.X.: 2002, A statistical study on the geoeffectiveness of Earth-directed coronal mass ejections from March 1997 to December 2000. *J. Geophys. Res.* **107**, 1340. DOI. ADS.

Webb, D.F., Cliver, E.W., Crooker, N.U., Cry, O.C.S., Thompson, B.J.: 2000, Relationship of halo coronal mass ejections, magnetic clouds, and magnetic storms. *J. Geophys. Res.* **105**, 7491. DOI. ADS.

Xu, D., Chen, T., Zhang, X.X., Liu, Z.: 2009, Statistical relationship between solar wind conditions and geomagnetic storms in 1998 – 2008. *Planet. Space Sci.* **57**, 1500. DOI. ADS.

Xystouris, G., Sigala, E., Mavromichalaki, H.: 2014, A complete catalogue of high-speed solar wind streams during solar cycle 23. *Solar Phys.* **289**(3), 995. DOI.

Yakovchouk, O.S., Mursula, K., Holappa, L., Veselovsky, I.S., Karinen, A.: 2012, Average properties of geomagnetic storms in 1932 – 2009. *J. Geophys. Res.* **117**, A03201. DOI. ADS.

Zhang, J., Dere, K.P., Howard, R.A., Bothmer, V.: 2003, Identification of solar sources of major geomagnetic storms between 1996 and 2000. *Astrophys. J.* **582**, 520. DOI. ADS.

Zhang, J., Richardson, I.G., Webb, D.F., Gopalswamy, N., Huttunen, E., Kasper, J.C., Nitta, N.V., Poomvises, W., Thompson, B.J., Wu, C.-C., Yashiro, S., Zhukov, A.N.: 2007, Solar and interplanetary sources of major geomagnetic storms ($Dst \leq -100$ nT) during 1996 – 2005. *J. Geophys. Res.* **112**(A11), A10102. DOI. ADS.

Zhang, X.-Y., Moldwin, M.B.: 2014, The source, statistical properties, and geoeffectiveness of long-duration southward interplanetary magnetic field intervals. *J. Geophys. Res.* **119**, 658. DOI. ADS.

Zhao, X.P., Webb, D.F.: 2003, Source regions and storm effectiveness of frontside full halo coronal mass ejections. *J. Geophys. Res.* **108**, 1234. DOI. ADS.